ISSN (Print) 1226-1750
ISSN (Online) 2233-6656
Journal of Magnetics 26(1), 129-140 (2021) https://doi.org/10.4283/JMAG.2021.26.1.129

Novel Scientific Simulations (Finite Element Method) for Peristaltic Blood Flow in an Asymmetric Channel: Applications of Magnetic and Inertial Forces

Wei-Mao Qian[1], Bilal Ahmed[2], Sami Ullah Khan[3], M. Ijaz Khan[4], and Abdul Haleem Hamid[5]*

[1]School of Continuing Education, Huzhou Vocational & Technical College, Huzhou 313000, P. R. China
[2]Department of Mathematics and Statistics, The University of Lahore, Sargodha Campus 40100, Pakistan
[3]Department of Mathematics, COMSATS University, Islamabad, Sahiwal 57000, Pakistan
[4]Department of Mathematics and Statistics, Riphah International University I-14, Islamabad 44000, Pakistan
[5]Department of Mathematics, Division of Science and Technology, University of Education, Lahore 54770, Pakistan

(Received 3 February 2021, Received in final form 20 March 2021, Accepted 23 March 2021)

Background: Recently, an utmost attention has been devoted by researchers on the prestaltic movement of viscous flows due to its novel importance in daily life problems, human body and many physical systems. In era of biological systemns and health sciences, the prestaltic mechanism attribute impotant applications blood circulation in vessels, blood pumping in heart, food in esophagus etc. Moreover, the applications of novel Galerkin finite element scheme for solution of nonlinear partial differential equations associated with peristaltic flow problems is another challenging task for mathematicians. Owing to such motivativations in mind, this computational presents the magnetohydrodynamic peristaltic flow of viscous fluid at high Reynolds number induced by an asymmetric wall channel. The novel impact of magnetic force are also utilized as a novelty. Method: The equations which exploit the flow problem are numerically tackled with help of Galerkin finite element scheme. Results: The results are computed and show great validation for physical parameters like wave constants, amplitude ratio and Reynolds number. The validation of obtained results are worked out with already claimed data and achieved an excellent accuracy. The mechanisms of transport process is addressed in view of involved physical parameters namely wave constant, Reynolds number and Hartmann number. The graphical observations are successfully revealed for all parameters.

Keywords : peristaltic flow, asymmetric channel, MHD flow, finite element method

1. Introduction

The phenomenon of peristalsis utilizes much dynamic significance in the era of various industries and physiological systems. The applications of peristaltic process in physiological system include flow of bold in arteries, urine movement from kidney to bladder, movement of blood in vessels, nutriment swallowing in esophagus etc. Moreover, flow encountered by roller pumps and pharmacological delivery arrangement also conveys applications of peristaltic transport. The indispensable theoretical analysis on the peristaltic pattern was organized by Latham [1]. Yung and Yih [2] followed the work based on the peristaltic analysis encountered by a fixed frame of reference without applications of lubrication theory. Shaprio *et al.* [3] deduct the mathematical relations for peristaltic movement of fluid based on the novel assumptions of low Reynolds number. The analysis reveals that upon consideration of long wavelength approach, the inertial features cannot play a justified role. This investigation provides a direction for researchers to conduct research on this topic with analytical approach, numerical simulations under various physical situations [4-11].

The investigations conducted above report the peristaltic pattern induced by tube or symmetric channels. The lubrication approach was pursued for presenting the mathematical relations for these useful investigations. The work performed by Mishra and Rao [18] directed the peristaltic movement of Newtonian material configured by an asymmetric channel in view of diverse amplitude ratio and phase shift. The dynamic mechanism of long wavelength postulation and inertia impact has been ignored for suggesting the mathematical model. An important claim reported in this analysis argues that flux

*Corresponding author: Tel: +92-300-9019713
Fax: +92-335-9761475, e-mail: mikhan@math.qau.edu.pk

rate and trapping zone are more progressive in symmetric channel in contrast to the asymmetric boundary channel. The importance of curvature features in viscous material followed the peristaltic mechanism has been worked out by Rao and Mishra [19]. Elshehawey *et al.* [20] modeled the peristaltic motion model confined a porous walls channel for viscous material flow in view of dominant wavelength hypothesis. Moreover, the inertial forces cannot play contributory role in this peristaltic approach. The solution structure was provided by using Adomian decomposition technique. The heat transportation in peristaltic study of viscous fluid induced by vertical channel having porous walls was led by Srinivas and Gayathri [21]. Ali and Hayat [22] deals with modeling of non-Newtonian fluid in peristaltic movement confined by asymmetric walls channel with variation of amplitude ratio. They concluded that increase in amplitude ratio of upper and lower wall increases pressure in pumping section. However, declining observations were searched out in co-pumping area. Later on varius approaches were made regarding analytical assumption of peristaltic movement in asymmetric channel owing to high wavelength consideration and small Reynolds number assumptions. The numerical solution of peristaltic motion against inertial effecton asymmetric channel is yet tooinvestigated. Only few studies can be seen in literatures recent past years for symmetric channel against Newtonian and Non-Newtonian fluid. Javed *et al.* [29] presented the numerical solution of MHD peristaltic motion at high Reynolds number of viscous fluids in an inclined channel. They used finite element method to solve the governing equation in symmetric channel for arbitrary values of amplitude ratio and wave number. They concluded that the size of trapping bolus increases by increasing Reynoldsand Hartmann numbers. They also described that the velocity is less sensitive in the range $0 \le Re \le 20$. Hamid *et al.* [30] studied the peristaltic motion of Non-Newtonian fluid in a symmetric channel. They also used finite element method toobtain the numerical solution and concluded that the pressure rise increases due to by increase in Reynolds and wave numbers. Asha and Deepa [31] evaluated the peristaltic mechanism of magnetized micropolar nanomaterial subject to the thermal radiation and entropy generation applications. The peristaltic analysis for the Rabinowitsch fluid model impacting chemical reactions and thermal radiation confined by flexible channel has been conducted by Imran *et al.* [32]. Vaidya *et al.* [33] modeled and analyzed a peristaltic flow problem form Jeffrey nanofluid confined by a porous tapered channel with wall transport features. Rashid *et al.* [34] investigated the peristaltic transport of Williamson fluid configured by a curved channel with external impact of magnetic force. Imran *et al.* [35] presented an investigation based on peristaltic motion in Jeffrey six constant in presence of nanofluid along a vertical non-uniform tube. Some other important research regarding fluid flow is listed in Refs. [36-45].

The aim of the present study is to investigate the numerical analysis of MHD peristaltic motion in asymmetric channel without using any assumption which will be valid for arbitrary Reynolds number.The current study extends the previous analysis carried out by Mishra and Rao [18], for the specified valueso of wave constant and Reynolds number. The invertigation performed by Mishra and Rao [18] declared analytical solution of asymmetric peristaltic flow under the assumption of low Reynolds number and long wavelength. The current study discussed the Reynolds number and wave number effects at different phase difference without using any assumption. This study also compared with the analytical solution of Mishra and Rao [18] as a limiting case for validation of the present results and found an excellent agreement.

2. Problem Formulation

Let us develope the mathematical model for peristaltic motion of viscous fluid subject to the magnetic force effects. The flow is confined by an infinite 2-D channel with width $2h_0$ as sketched in Fig. 1. The magnetic force impact is assumed along normal direction of flow. The imposed magnetic force has uniform strength of magnetic field represented with B_0. The origin of flow is based on movement of wave train having velocity c in the channel direction which is denoted by following relations:

$$H_1(X, t) = h_0 - d_1^* \cos\left\{\frac{2\pi(X - ct)}{\lambda}\right\}, \qquad \text{(Upper wall)} \tag{1}$$

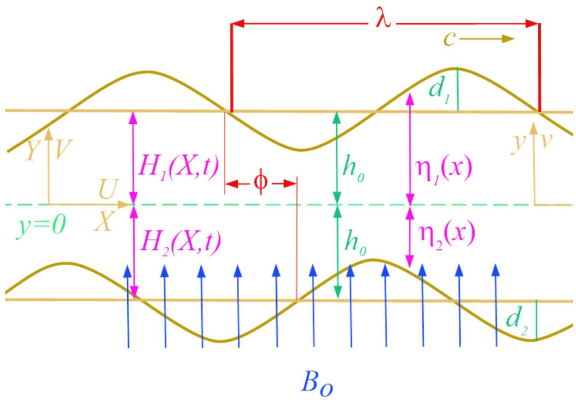

Fig. 1. (Color online) Geometry of two-dimensional peristalticasymmetric channel.

$$H_2(X, t) = -h_0 + d_2^* \cos\left\{\frac{2\pi(X - ct)}{\lambda} + \phi\right\}, \text{ (lower wall)} \quad (2)$$

with physical quantities λ (wavelength), d_1^*, d_2^* (wave amplitudes) and ϕ (phase difference in peristaltic waves). The value of ϕ is taken from [0, π]. It is remarked that results for symmetric channel in absence of phase wave are achieved when $\phi = 0$. The imposed relations in fixed frame are structured as:

$$\frac{\partial U}{\partial x} + \frac{\partial V}{\partial Y} = 0, \quad (3)$$

$$\rho\left(\frac{\partial U}{\partial t} + U\frac{\partial U}{\partial X} + V\frac{\partial V}{\partial Y}\right) = -\frac{\partial P}{\partial X} + \mu\left(\frac{\partial^2 U}{\partial X^2} + \frac{\partial^2 U}{\partial Y^2}\right) - \sigma B_0^2 U, \quad (4)$$

$$\rho\left(\frac{\partial V}{\partial t} + U\frac{\partial V}{\partial X} + V\frac{\partial V}{\partial Y}\right) = -\frac{\partial P}{\partial Y} + \mu\left(\frac{\partial^2 V}{\partial X^2} + \frac{\partial^2 V}{\partial Y^2}\right), \quad (5)$$

Above relations are imposed in fixed frame where U reflects the velocity components along the direction of X while the velocity components specified along Y is symbolized with V.

$$U = 0,\ V = \frac{\partial H_1}{\partial t} \text{ at } Y = H_1, \quad (6)$$

$$U = 0,\ V = \frac{\partial H_2}{\partial t} \text{ at } Y = H_2. \quad (7)$$

The boundary conditions on $U = 0$ at $Y = H_1$ and $Y = H_2$ arises no-slip at the upper and lower wall respectively. The condition $V = \frac{\partial H_1}{\partial t}$ at Y = H_1 and $V = \frac{\partial H_2}{\partial t}$ at $Y = H_2$ shows that the normal velocity of fluid at the upper and lower walls is equal to the normal wall velocity respectively. The transformation relating the laboratoryframe to waveframe isdefine as

$$x' = X - ct,\ y' = Y,\ u' = U - c,\ v' = V,\ p' = P, \quad (8)$$

where (u', v') are x' and y' components of velocity in moving frame, respectively.Introducing the following dimensionless variables

$$x = \frac{x'}{\lambda},\ y = \frac{y'}{h_0},\ u = \frac{u'}{c},\ v = \frac{v'}{c},\ d_1 = \frac{d_1^*}{h_0},\ d_2 = \frac{d_2^*}{h_0},$$

$$\alpha = \frac{h_0}{\lambda},\ q = \frac{q'}{h_0},\ p = \frac{h_0^2}{\lambda c \mu}p'(x'),\ \eta_1(x) = \frac{H_1(x')}{h_0},$$

$$\eta_2(x) = \frac{H_2(x')}{h_0},\ \psi = \frac{\psi'}{ch_0},\ \omega = \frac{\omega'}{c/h_0}. \quad (9)$$

The dimensionless form of governing equation and boundary conditions in moving frame can be written as

$$\frac{\partial u}{\partial x} + \frac{\partial v}{\partial y} = 0, \quad (10)$$

$$Re\left(\alpha u\frac{\partial u}{\partial x} + v\frac{\partial u}{\partial y}\right) = -\frac{\partial p}{\partial x} + \left(\alpha^2\frac{\partial^2 u}{\partial x^2} + \frac{\partial^2 u}{\partial y^2}\right) - M^2(u + 1), \quad (11)$$

$$\alpha Re\left(\alpha u\frac{\partial v}{\partial x} + v\frac{\partial v}{\partial y}\right) = -\frac{\partial p}{\partial y} + \alpha\left(\alpha^2\frac{\partial^2 u}{\partial x^2} + \frac{\partial^2 u}{\partial y^2}\right), \quad (12)$$

$$u = -1,\ v = 2\pi d_1 \sin(2\pi x) \text{ at } y = \eta_1(x), \quad (13)$$

$$u = -1,\ v = 2\pi d_2 \sin(2\pi x + \phi) \text{ at } y = \eta_2(x), \quad (14)$$

where

$$\eta_1(x) = 1 - d_1\cos(2\pi x) \text{ and}$$
$$\eta_2(x) = 1 - d_2\cos(2\pi x + \phi), \quad (15)$$

where $Re = ca\alpha/\nu$ is the Reynolds number which represents the ratio of inertial forces to the viscous forces, α is the wave number, $M = (\sqrt{\phi/\mu}B_0\alpha)\alpha/\lambda$ is the Hartmann number represents the ratio of the electromagnetic force to the viscous force and $\eta_1(x) = 1 - d_1\cos(2\pi x)$ and $\eta_2(x) = -1 + d_2\cos(2\pi x + \phi)$ represents dimensionless form of upper and lower walls respectively, where d_1 is the amplitude ratio of upper wall and d_2 is the amplitude ratio of lower wall. Upon introducing the stream function ψ and vorticity ω defined by

$$u = \frac{\partial \psi}{\partial y},\ v = \alpha\frac{\partial \psi}{\partial x},\ \omega = \alpha\frac{\partial v}{\partial x} - \frac{\partial u}{\partial y}, \quad (16)$$

in Eqs. (11) and (12), after eliminating pressure terms,we get

$$\alpha^2\frac{\partial^2 \psi}{\partial x^2} + \frac{\partial^2 \psi}{\partial y^2} = -\omega, \quad (17)$$

$$Re\left(\frac{\partial \psi}{\partial y}\frac{\partial \omega}{\partial x} - \frac{\partial \psi}{\partial x}\frac{\partial \omega}{\partial y}\right) = \nabla^2\omega + M^2\frac{\partial^2 \psi}{\partial y^2}. \quad (18)$$

The corresponding boundary conditions on wall in term of ψ are [18]

$$\psi = \frac{q}{2},\ \frac{\partial \psi}{\partial y} = -1,\ \frac{\partial \psi}{\partial x} = 2\pi d_1 \sin(2\pi x) \text{ at } y = \eta_1(x), \quad (19)$$

$$\psi = \frac{q}{2},\ \frac{\partial \psi}{\partial y} = -1,\ \frac{\partial \psi}{\partial x} = -2\pi d_2 \sin(2\pi x + \phi) \text{ at } y = \eta_2(x) \quad (20)$$

where

$$\nabla^2 = \alpha^2\frac{\partial^2}{\partial x^2} + \frac{\partial^2}{\partial y^2}. \quad (21)$$

3. Finite Element Analysis

The peristaltic pattern of viscous material has been mathematically modeled in set of Eqs. (17) and (18) along with the boundary assumptions defined in Eqs. (19-20). These expressions are of partial in nature for which computation of solution is main task in this section. On this end, finite element technique, a famous numerical approach is followed to achieve the numerical simulations. The mesh point for this solution technique is suggested with appliance of built-in pdetool function with help of MATLAB computational software. In many reported research on this topic, the modeling of such peristaltic problems are tackled low Reynolds number and long wavelength assumptions. The novel objective of this attempt is to involve the influence of such prime quantities to perform the analysis. The highly convincing numerical iterations are achieved by following the quadratic triangle elements. The approximated stream function and vorticity are suggested via following relations:

$$\psi = \Sigma_{k=1}^{n} N_k \psi_k, \ \omega = \Sigma_{k=1}^{n} N_k \omega_k, \tag{22}$$

with element nodal approximations ω_k which associated with ω and ψ_k with ψ. Moreover, N_k represents the element node shape function. With help of following Galerkin's formulation are imposed:

$$\int_\Omega w_1 \left(\alpha^2 \frac{\partial^2 \psi}{\partial x^2} + \frac{\partial^2 \psi}{\partial y^2} + \omega \right) d\psi d\omega = 0, \tag{23}$$

$$\int_\Omega w_2 \left(Re \left(\frac{\partial \psi}{\partial y}\frac{\partial \omega}{\partial x} - \frac{\partial \psi}{\partial x}\frac{\partial \omega}{\partial y} \right) - \left(\alpha^2 \frac{\partial^2 \omega}{\partial x^2} + \frac{\partial^2 \omega}{\partial y^2} \right) - M^2 \left(\alpha^2 \frac{\partial^2 \psi}{\partial y^2} \right) \right) d\psi d\omega = 0, \tag{24}$$

where w_1 and w_2 are weight functions and Ω is domain of the problem. After simplification, the Eqs. (23) and (24) can be written as:

$$\int_\Omega \left(\alpha^2 \frac{\partial w_1}{\partial x}\frac{\partial \psi}{\partial x} - \frac{\partial w_1}{\partial y}\frac{\partial \psi}{\partial y} + w_1 \omega \right) d\psi d\omega = \int_\Gamma w_1 \frac{\partial \psi}{\partial n} d\Gamma, \tag{25}$$

$$\int_\Omega Re w_2 \left(\frac{\partial \psi}{\partial y}\frac{\partial \omega}{\partial x} - \frac{\partial \psi}{\partial x}\frac{\partial \omega}{\partial y} \right) d\psi d\omega + \int_\Omega \left(\alpha^2 \frac{\partial w_2}{\partial x}\frac{\partial \omega}{\partial x} + \frac{\partial w_2}{\partial y}\frac{\partial \omega}{\partial y} \right) d\psi d\omega + M^2 \int_\Omega \frac{\partial w_2}{\partial y}\frac{\partial \psi}{\partial y} d\psi d\omega = \int_\Gamma w_2 \frac{\partial \omega}{\partial n} d\Gamma + M^2 \int_\Gamma w_2 \frac{\partial \psi}{\partial n} d\Gamma, \tag{26}$$

where Γ is boundary of the domain. After introducing Eq. (22) into Eqs. (25) and (26) and considering the discretized domain, we have:

$$-\Sigma_i B_{ki}^e \omega_i + \Sigma_i A_{ki}^e \psi_1 = S_n^{k^e}, \tag{27}$$

$$\Sigma_i A_{ki}^e \omega_i + Re \ \Sigma_{i,j} C_{kij}^e \psi_i \omega_i = M^2 \Sigma_i D_{ki}^e \psi_i = M^2 S_n^{k^e}, \tag{28}$$

with B_{ki}^e (mass matrix), A_{ki}^e, C_{kij}^e (convective matrix), $S_n^{k^e}$ (force vector) with following definition:

$$A_{ki}^e = \int_{\Omega^e} \left(\alpha^2 \frac{\partial P N_k}{\partial x}\frac{\partial N_i}{\partial x} + \frac{\partial N_k}{\partial y}\frac{\partial N_i}{\partial y} \right) d\Omega^e, \tag{29}$$

$$B_{ki}^e = \int_{\Omega^e} N_k N_i d\Omega^e, \tag{30}$$

$$C_{kij}^e = \int_{\Omega^e} N_k \left(\frac{\partial N_i}{\partial y}\frac{\partial N_j}{\partial x} - \frac{\partial N_j}{\partial x}\frac{\partial N_i}{\partial y} \right) d\Omega^e, \tag{31}$$

$$D_{ki}^e = \int_{\Omega^e} \frac{\partial N_k}{\partial y}\frac{\partial N_i}{\partial y} d\Omega^e, \tag{32}$$

$$S_n^{k^e} = \int_\Gamma N_k \bar{S}_k d\Gamma, \tag{33}$$

The system of equations (27) and (28) combined as a global system in matrix form defined as

$$\boldsymbol{KA} = \boldsymbol{F}. \tag{34}$$

where

$$K_{ij} = \begin{bmatrix} B_{ki}^e & A_{ki}^e \\ A_{ki}^e & Re C_{kij}^e \omega_i + M^2 D_{ki}^e \end{bmatrix}, \ A_k = \begin{bmatrix} \omega_k \\ \psi_k \end{bmatrix},$$

$$F_k = \begin{bmatrix} S_n^{k^e} \\ M^2 S_n^{k^e} \end{bmatrix}. \tag{35}$$

The global matrix system formulated in Eq. (34) is numerically treated with Newton-Raphson technique upto excellent iterative accuract.

4. Pressure Evaluation

The contribution of pressure per unit length cannot be denied in peristaltic pattern flow problems. The change in pressure arise per unit length has been measured with applications of numerical integration of pressure gradient. The movement of peristaltic transport is referred to the infinite sinusoidal wave, therefore, the pressure is computed only at $y = 0$. The change in pressure gradient is imposed from Navier-Stokes relations as:

$$\frac{\partial p}{\partial x} = Re \left(\frac{\partial^2 \psi}{\partial y^2}\frac{\partial \psi}{\partial x} - \frac{\partial^2 \psi}{\partial x \partial y}\frac{\partial \psi}{\partial y} \right) - \frac{\partial \omega}{\partial y} - M^2 \left(\frac{\partial \psi}{\partial y} + 1 \right), \tag{36}$$

$$\frac{\partial p}{\partial x} = Re\alpha^2\left(\frac{\partial^2\psi}{\partial x^2}\frac{\partial\psi}{\partial y} - \frac{\partial^2\psi}{\partial x\partial y}\frac{\partial\psi}{\partial x}\right) - \alpha\frac{\partial\omega}{\partial y}, \tag{37}$$

The change in ΔP_λ is

$$\Delta P_\lambda = \int_0^\lambda \frac{\partial p}{\partial x}dx\,. \tag{38}$$

5. Result and Discussion

The boundary value problem (17) and (18) has been solved using finite element method by developing code in MATLAB. Figure 2 shows the validation of the present result with the existing result of Mishra and Rio [18] at low Reynolds and wave numbers assumption. It is observed that the present results are highly accurate and

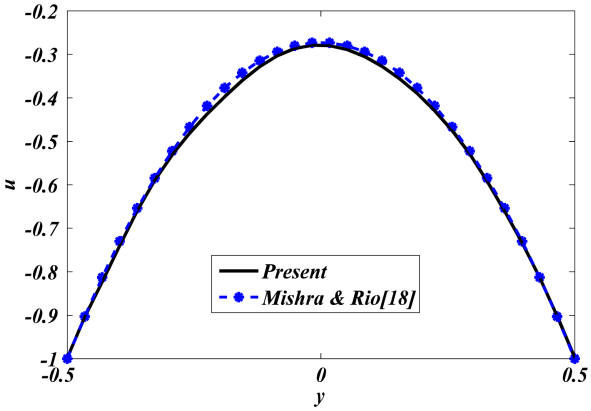

Fig. 2. (Color online) Comparison of velocity profile of present computational result with analytical solution of Mishra and Rio [18] at $Re = 0$, $\alpha = 0$ and $d_1 = d_2 = 0.5$.

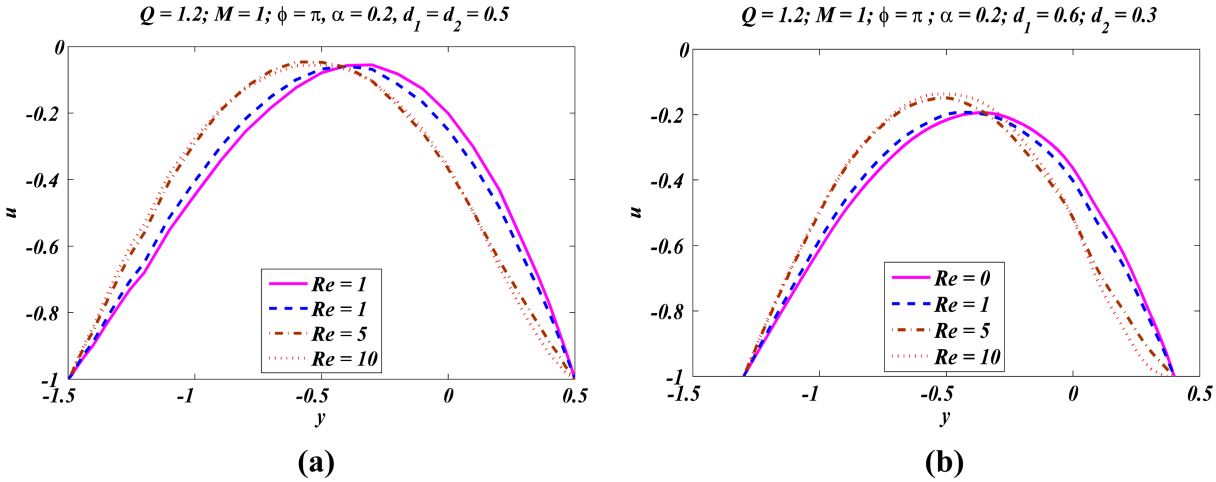

Fig. 3. (Color online) Velocity profiles for different Reynolds number (a) $M = 1$, $Q = 1.2$, $\phi = \pi$, $\alpha = 0.2$, $d_1 = d_2 = 0.5$, (b) $M = 1$, $Q = 1.2$, $\phi = \pi$, $\alpha = 0.2$, $d_1 = 0.6$, $d_2 = 0.3$.

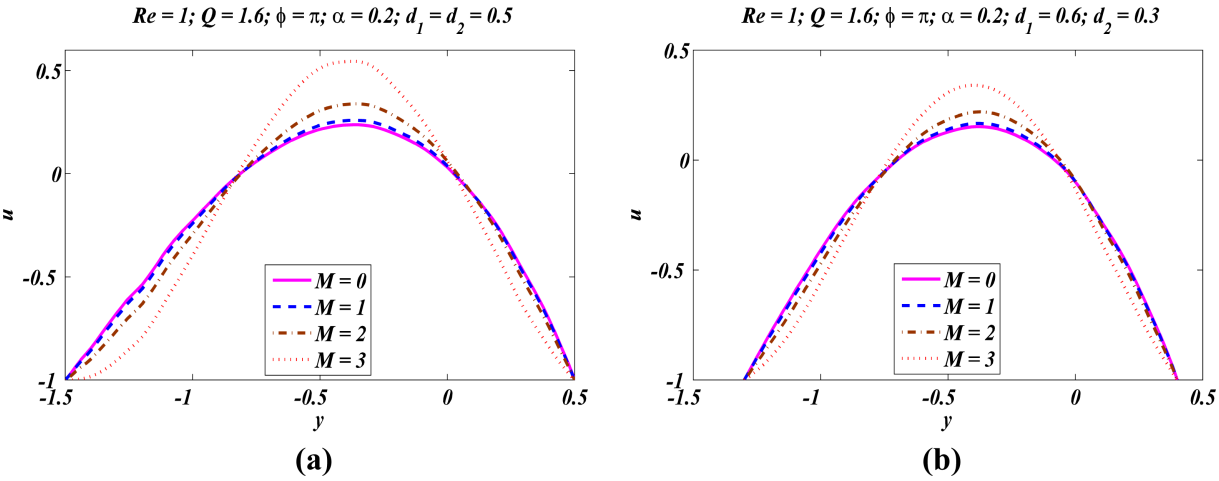

Fig. 4. (Color online) Velocity profiles for different Hartmann number (a) $Re = 1$, $Q = 1.6$, $\phi = \pi$, $\alpha = 0.2$, $d_1 = d_2 = 0.5$, (b) $Re = 1$, $Q = 1.6$, $\phi = \pi$, $\alpha = 0.2$, $d_1 = 0.6$, $d_2 = 0.3$.

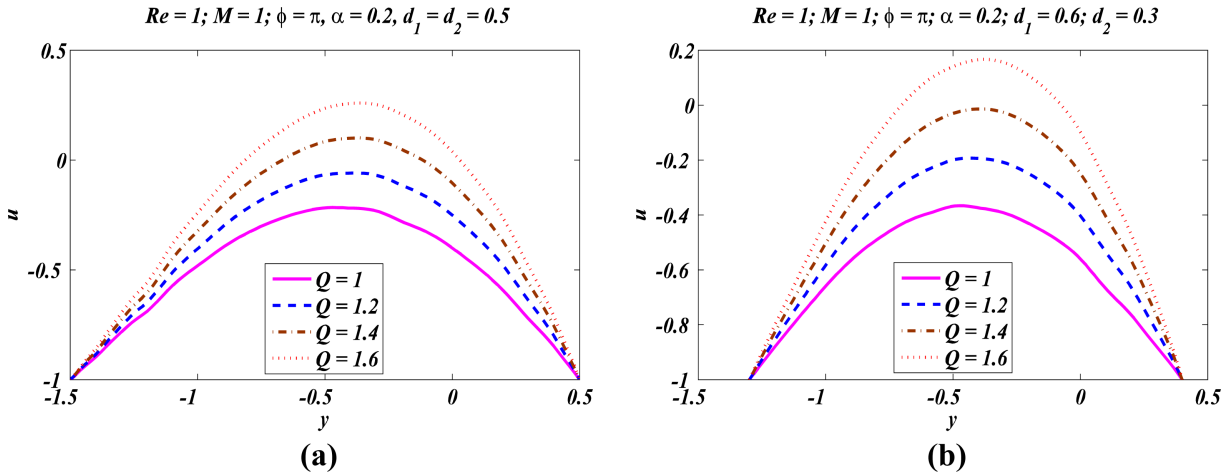

Fig. 5. (Color online) Velocity profiles for different time mean flow rate (a) Re = 1, M = 1, $\phi = \pi$, α = 0.2, $d_1 = d_2$ = 0.5, (b) Re = 1, M = 1, $\phi = \pi$, α = 0.2, d_1 = 0.6, d_2 = 0.5.

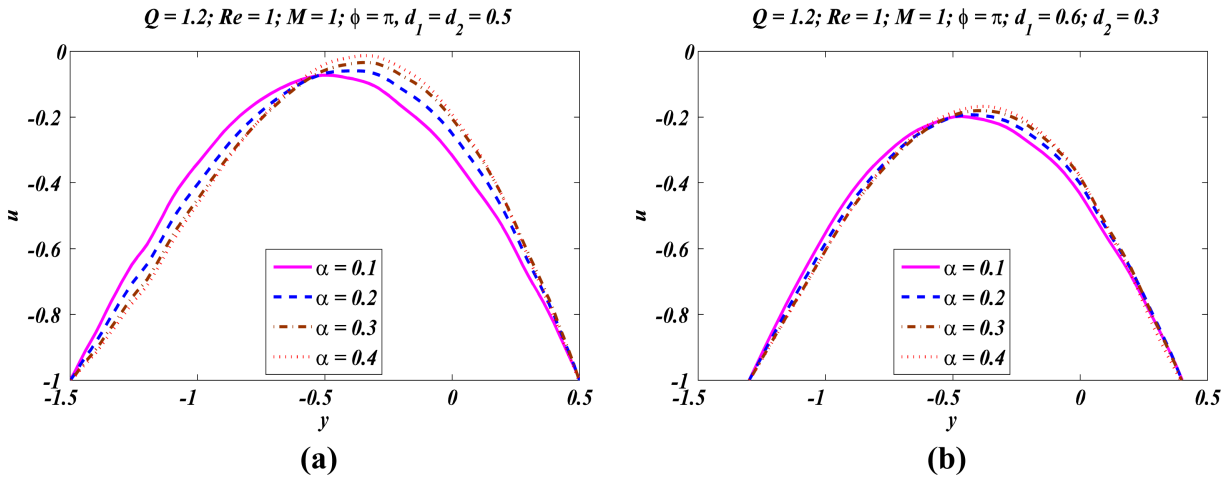

Fig. 6. (Color online) Velocity profiles for different wave number (a) Re = 1, Q = 1.6, $\phi = \pi$, M = 1, $d_1 = d_2$ = 0.5, (b) Re = 1, Q = 1.6, $\phi = \pi$, M = 1, d_1 = 0.6, d_2 = 0.3.

well matched with the result of Mishra and Rio [18]. It validates that the formulation and simulation presented is also valid for high Reynolds and wave numbers. The velocity profiles against different values of Re, M, Q and α are plotted in Figs. 3-5. All the results are plotted at phase difference $\phi = \pi$, amplitude ratio $d_1 = d_2$ = 0.5 and d_1 = 0.6, d_2 = 0.3. Figure 3 shows the velocity profile for different values of Reynolds number at fixed values of M = 1 and Q = 1.6. It is noted that with increasing Reynolds number, velocity profile decreases near the upper wall and increasing near the lower wall. It is also noticed that, the velocity increases at center of the channel due to increase in Reynolds number up to 10 at amplitude ratio d_1 = 0.6 for upper wall and d_2 = 0.3 for lower wall. It concludes that at different amplitude ratio, velocity decreases with increasing Reynolds number. The velocity profiles at different value of Hartmann number (M) is shown in Fig. 4 with fixed Q = 1.6 and Re = 1. A rapid increment in velocity associated with the center part of channel is evaluated with dominant variation of Hartmann number and decreases near both the upper and lower walls of the channel. Moreover, the velocity reduces when amplitude ratio of upper and lower walls are different. Figure 5 shows the velocity profile for different value mean flow rate. The observations claimed that by increasing time mean flow rate Q, the velocity increases throughout the region. Moreover, the velocity increases at center part of the channel if the amplitude ratio of upper and lower walls are same. The velocity profile against differentwave number α is plotted in Fig. 6. It is noted that with increasing wave number, the velocity decreases at lower part of the wave. These effects are observed

reversed at upper section of the wave, that is, velocity increases near the upper wall by increasing wave number. It concludes that fluid velocity is faster in upper section of the channel as compared to that of lower channel. It is also observed that velocity enhanced whenamplitude ratio of upper and lower walls are maintained same and reduced

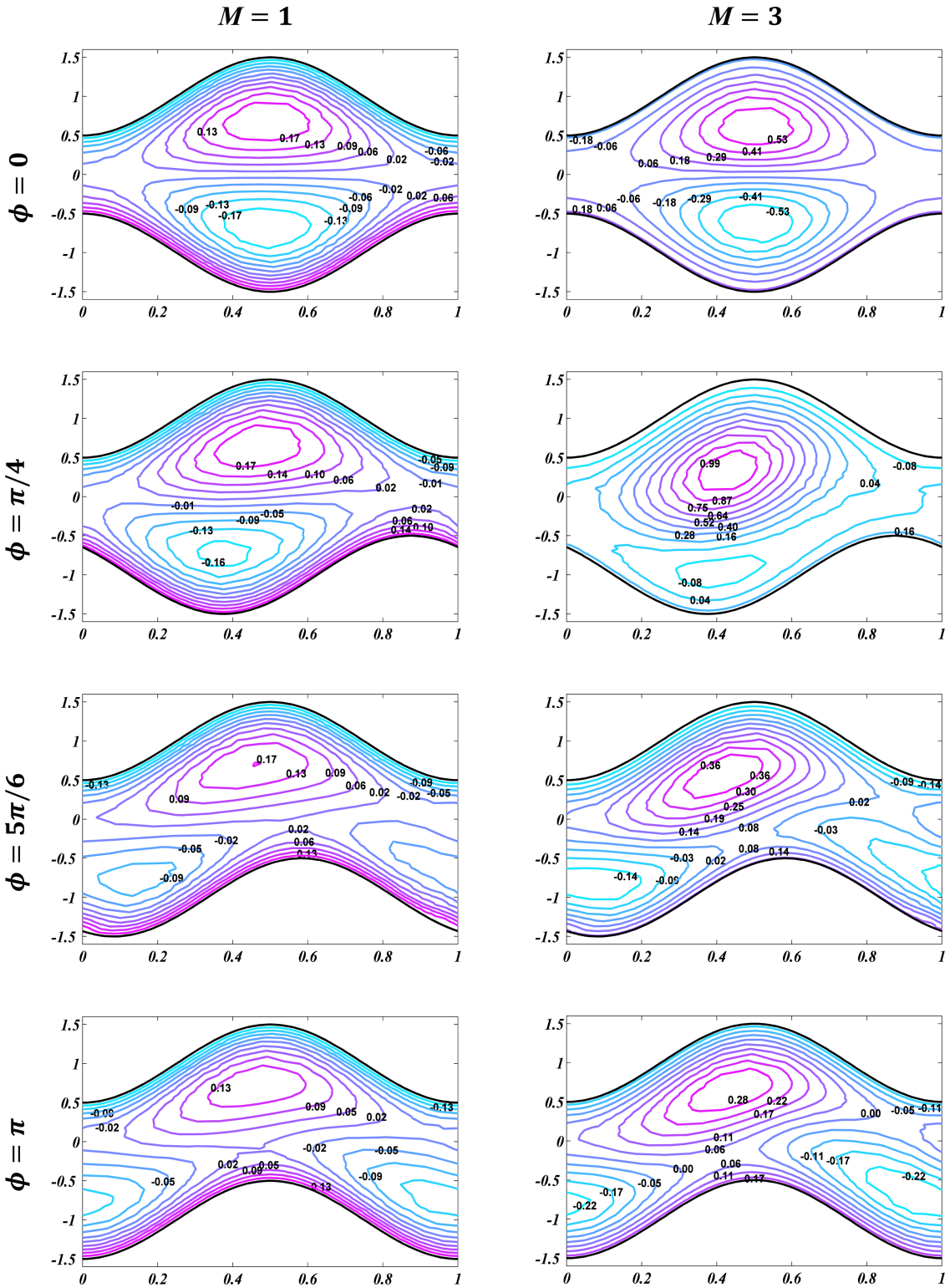

Fig. 7. (Color online) Streamline against different phase shift for $M = 1$ (left) and $M = 3$ (right) with fixed parameter $Q = 1.6$, $Re = 1$, $d_1 = d_2 = 0.5$.

when amplitude ratio is different against all parameters. It accomplishes that amplitude ratio plays an important role in reduction/enhancement of fluid velocity.

The streamline structure in wave frame is similar to the walls because the walls are assumed to be stationary. However, in diverse situations the shape of streamline

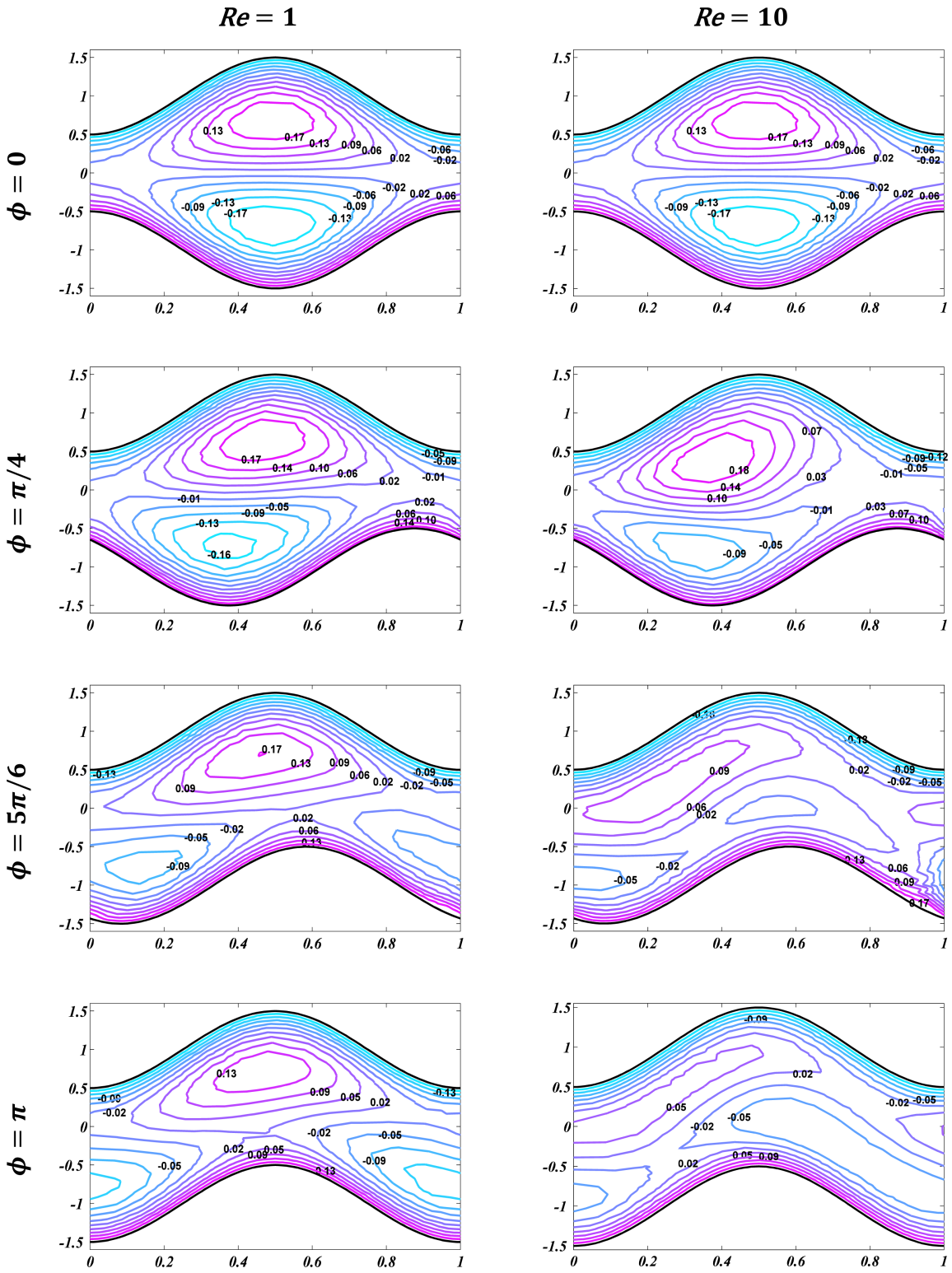

Fig. 8. (Color online) Streamline against different phase shift for Re = 1 (left) and Re = 1 (right) with fixed parameter Q = 1.6, M = 1, d_1 = d_2 = 0.5.

split to enclose bolus of fluidparticles in closedstreamlines which is called trapping phenomenon. Figures 7 to 9 shows the trapping behavior for different value of M, Re and Q at phase differences $\phi = 0$ (symmetric flow), $\phi = \pi/4$, $\phi = 5\pi/6$ and $\phi = \pi$. Figure 7 shows the trapping phenomena for Hartmann number $M = 1$ and $M = 3$ with

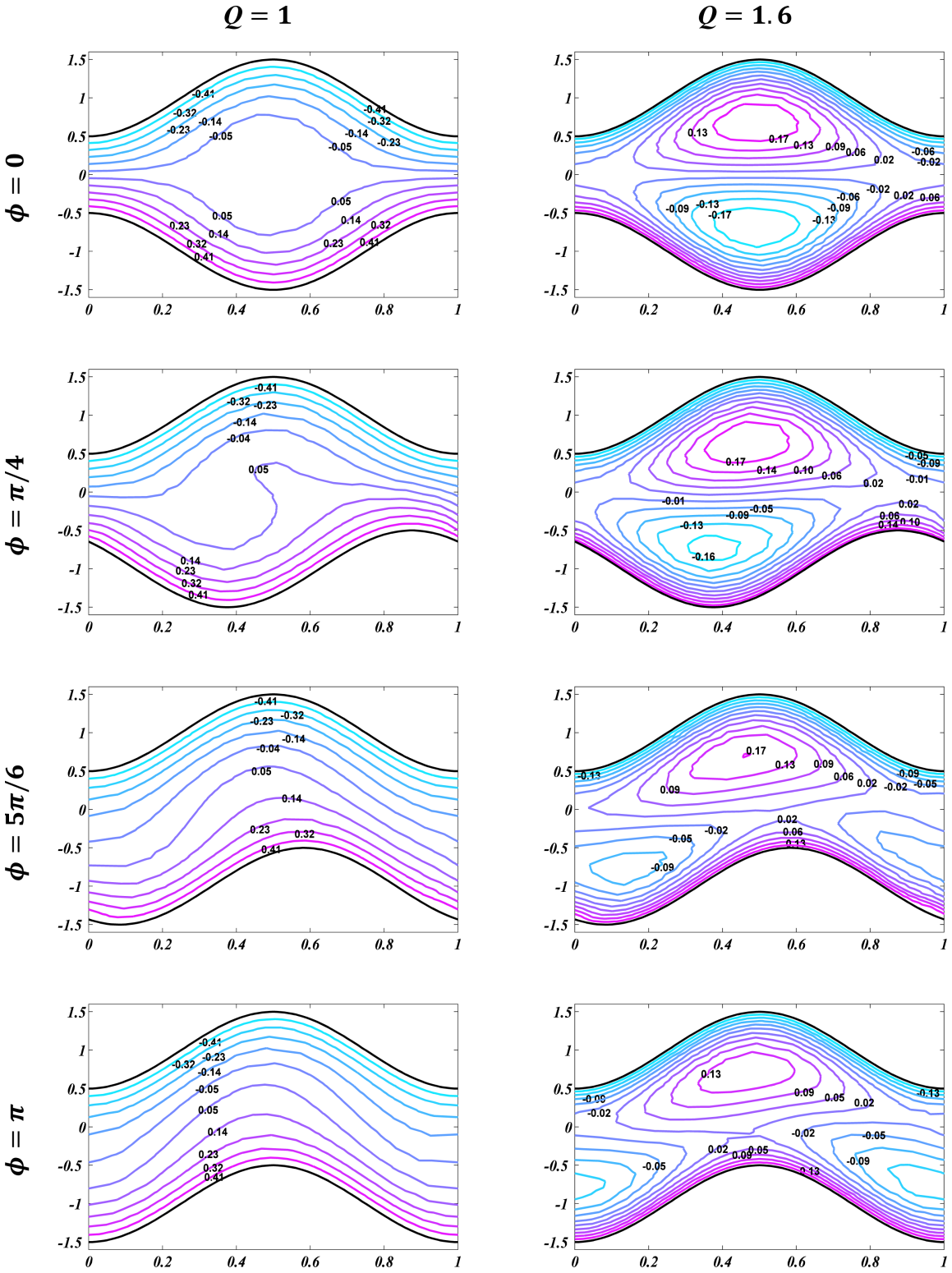

Fig. 9. (Color online) Streamline against different phase shift for $Q = 1$ (left) and $Q = 1.6$ (right) with fixed parameter $Re = 1$, $M = 1$ and $d_1 = d_2 = 0.5$.

same amplitude $d_1 = d_2 = 0.5$ for both upper and lower walls. It is observed that for small value of Hartmann number, the size of boluses decreases near the upper wall against any phase difference. The size of bolus decreases near the lower wall when phase difference $\phi \leq 5\pi/6$ and increases when $\phi \geq 5\pi/6$. It is also observed that the trapping bolus near the lower wall move along the wall, but when Hartmann number $M = 3$, the size of bolus increases near the upper wall at phase difference $\phi \leq \pi/4$ and then decreases when phase difference $\phi > \pi/4$. Moreover, the size of bolus increases at large Hartmann number as compare to small Hartmann number for different phase shift in the upper surface of channel wall. The conclusion point out from such results reveal that phase difference ϕ may useful to depress the fluid velocity at small Hartmann number. Also, large Hartmann number helps to increase velocity at the center part of the channel. Figure 8 shows the trapping phenomena for $Re = 1$ and $Re = 10$. It is observed that the size of trapping bolus reduces near the upper wall against small inertial forces, but when inertial force increases, the size of trapping bolus first increases and then decreases by increasing phase difference ϕ. It is also seen that, there is no significant effects are observed in symmetric channel against large value of Reynolds number. An interesting point is noted that the more bolus appear in the upper section of the channel as compare to that of the lower section when phase difference is $\phi = \pi/4$ and $\phi = 5\pi/6$ for large Reynolds number. It means that the velocity of the fluid is higher near the upper wall while velocity reduces near the lower wall. When $\phi = \pi$ and $Re = 10$, the trapping boluses get reduces and moving along the walls. Figure 9 shows the streamlines against time mean flow rate at $Q = 1$ and $Q = 1.6$. It is noted that for small value of Q, the streamlines look same as the lower and upper wall while when Q increase, the trapping boluses are formed. It is observed that the size of trapping boluses decreases near the upper wall at different phase difference. It is also noted that the trapping bolus initially decreases near the lower wall when phase difference is $\phi \leq 5\pi/6$ and then increases when phase difference become $\phi > 5\pi/6$.

Pressure rise ΔP_λ per wavelength is the important characteristic in peristaltic pumping which gives the idea of flow rate in the flow field. Figures 10 to 15 show the variation of pressure rise per wave length against time mean flow for different value of Reynolds number (Re), Hartmann number (M), wave number (α), phase difference (ϕ) and different amplitude ratios respectively.In these Figures, it is seen that the free pumping $\Delta P_\lambda = 0$ appear in the range of $0 \leq Q \leq 1.5$ against all the parameters. In

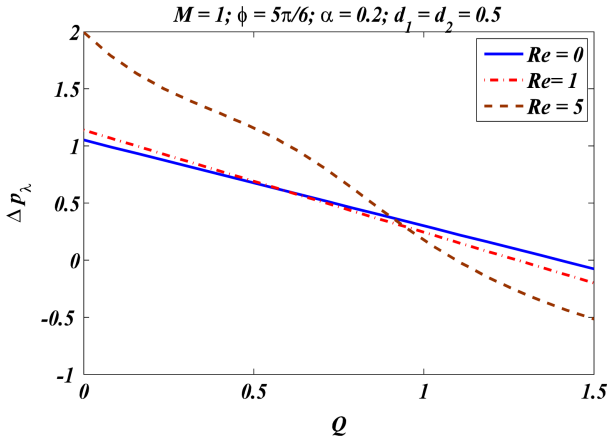

Fig. 10. (Color online) Pressure rise per wave length for Reynolds number (Re).

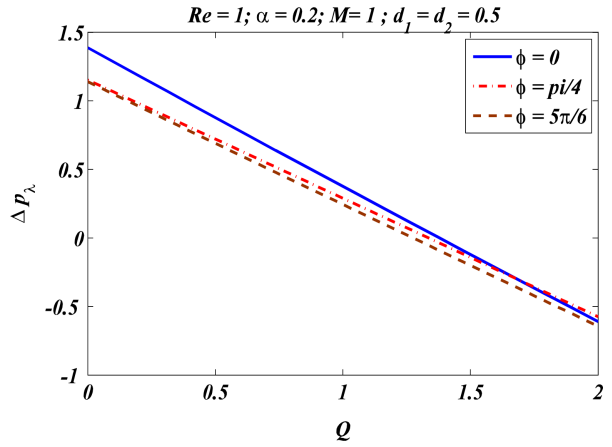

Fig. 11. (Color online) Pressure rise per wave length for Hartmann number (M).

Figure 10, it is observed that the pressure is linear for small inertial force but when inertial forces increase the

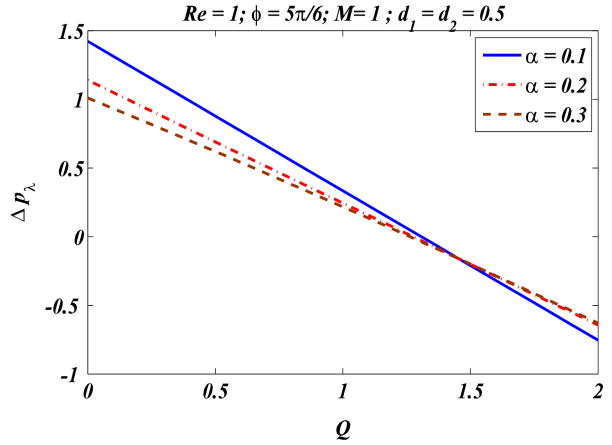

Fig. 12. (Color online) Pressure rise per wave length for wave number (α).

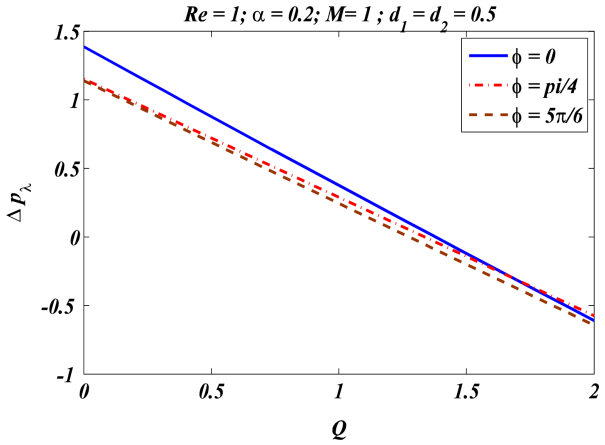

Fig. 13. (Color online) Pressure rise per wave length for phase difference (ϕ).

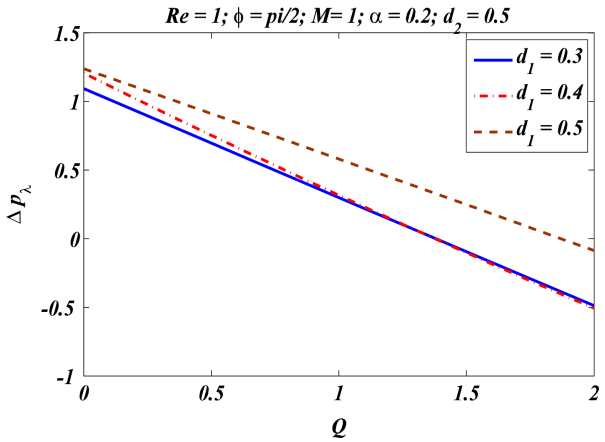

Fig. 14. (Color online) Pressure rise per wave length for different amplitude ratio of upper wall.

pressure rise per wave length is not linear. Also by increasing inertial forces the pressure enhance in the region of positive pumping while declining trend is credited in co-pumping area. The change in pressure against fluctuated values of Hartmann number against small inertial force and phase difference $\phi = 5\pi/6$ are shown Fig. 11. The profile of ΔP_λ is sufficiently progressive in pumping portion while is reduce in co-pumping region. A contrasted change in ΔP_λ is noticed for wav constant which is due to fact that, in wave number, the pressure decreases in positive pumping region and increases co-pumping region as illustrated in Fig. 12. Figure 13 shows the pressure rise per wave length against difference phase shift. It is observed that pressure is maximum in the case of symmetric channel (ϕ = 0) and decreases by increasing phase difference in positive pumping region. Pressure rise per wave length for different amplitude ratio for upper and lower walls are

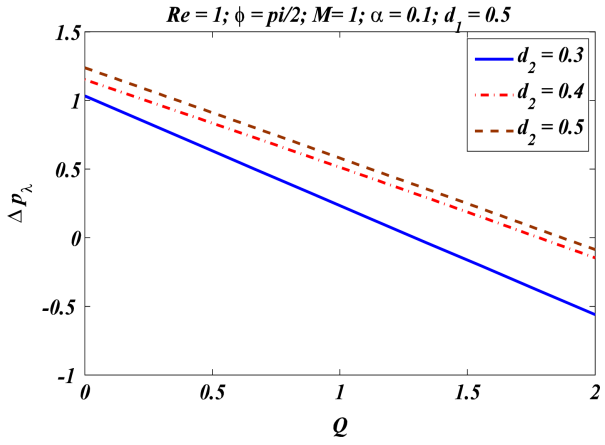

Fig. 15. (Color online) Pressure rise per wave length for different amplitude ratio of lower wall.

observed in Figs. 14 and 15 respectively. It is observed that pressure is linear and maximum on the same amplitude ratio of upper and lower wall. Further, pressure rise increases in positive pumping region when amplitude ratio of upper wall increases and depress in co-pumping surface. The another observations claimed here attribute that ΔP_λ is maximum when amplitude ratio subject ot lower channel wall get increase.

6. Conclusions

Computation study is carried out for two-dimensional peristaltic flow in the asymmetric channel without neglecting the inertial force and long wavelength assumptions. The finite elementtechnique is used to solve the governing higher order nonlinear equation. The graphical reflection of stream function, pressure distribution and longitudinal velocity against time are successfully presented. The results for these profiles are computed at lower surface and upper region of channel. The analysis reported without applications of small Reynolds number approach and consideration of long wavelength is comparatively different. The observations claimed from current continuation are summarized as:

- The longitudinal velocity increases at the center part of the channel by increasing the amplitude ratio of the upper and lower wall.
- The change in Hartmann number show a decrement in velocity near the channel wall while the trend at center is different.
- Th inertial forces are dominant over the viscous forces near the lower wall.
- The variation in wave constant improve the inertial impact which result a decrement in velocity at lower

channel surface. The size of trapped bolus increases for large Reynolds number, Hartmann number and phase difference and hence the velocity is maximum at high Reynolds number.

- The size of trapped bolus decreases when the phase difference is shifted to against Reynolds number, Hartmann number and time mean flow rate.
- The pressure rise is linear against small Reynolds number.
- The pressure enhances in pumping area with increasing Reynolds and Hartmann numbers. However, it decreases with increasing wave number and phase difference. Moreover, pressure rise per wavelength-achieves is maximum at same amplitude ratio of upper and lower walls.

References

[1] T. W. Latham, Master thesis, MIT, Massachusetts (1966).
[2] Y. C. Fung and C. S. Yih, Trans, ASMA. E. J. Appl. Mech. **35**, 669 (1968).
[3] A. H. Shapiro, M. Y. Jaffrin, and S. L. Weinberg, J. Fluid Mech. **37**, 799 (1969).
[4] M. Y. Jaffrin, Int. J. Eng. Sci. **11**, 681 (1973).
[5] A. M. Provost and W. H. Schwarz, J. Fluid Mech. **279**, 177 (1994).
[6] Kh. S. Mekheimer, Arb. J. S. and Eng. **28**, 183 (2003).
[7] Kh. S. Mekheimer, App. Math. and Comp. **153**, 763 (2004).
[8] N. Ali, M. Sajid, T. Javed, and Z. Abbas, Int. J. Heat and Mass Transfer. **53**, 3319 (2010).
[9] N. Ali, Q. Hussain, T. Hayat, and S. Asghar, Phy. Letter A **372**, 1477 (2008).
[10] D. Trapathi and O. Anwer Beg, Math. Biosciences **246**, 72 (2013).
[11] S. L. Weinberg, E. C. Eckistein, and A. H. Shapiro, J. Fluid Mech. **49**, 461 (1971).
[12] C. C. Yin and Y. C. Fung, J. Fluid Mech. **47**, 93 (1971).
[13] S. Takabatake and K. Ayukawa, J. Fluid Mech. **122**, 439 (1982).
[14] S. Takabatake, K. Ayukawa, and A. Mori, J. Fluid Mech. **193**, 267 (1988).
[15] S. Takabatake, K. Ayukawa, and M. Sawa, Japan. Society of Mech. Eng. **53**, 1207 (1989).
[16] S. Takabatake, Japan. Society of Mech. Eng. **56**, 3633 (1990).
[17] B. V. R. Kumar and K. B. Naidu, Comp. & Fluid **24**, 191 (1995).
[18] M. Mishra and A. R. Rao, Z. Angew. Math. Phys. **54**, 532 (2003).
[19] A. R. Rao and M. Mishra, Acta Mech. **168**, 35 (2004).
[20] E. F. Elshehawey, N. T. Eldabe, E. M. Elghazy, and A. Ebaid, App. Math. Comp. **182**, 140 (2006).
[21] S. Srinivas and R. Gayathri, App. Math. Comp. **215**, 185 (2009).
[22] N. Ali and T. Hayat, Comp. Math App. **55**, 589 (2008).
[23] M. Mishra and A. R. Rao, Int. J. Nonlinear Mach. **42**, 1153 (2007).
[24] S. Srinivas and V. Pushparaj, Comm. in Nonlinear Sci. and Numerical Simulation **13**, 1782 (2008).
[25] M. Kothandapani and S. Srinivas, Int. J. Non-Linear Mech. **43**, 915 (2008).
[26] N. Ali, T. Hayat, and M. Sajid, Biorheology **44**, 125 (2007).
[27] M. V. Subba Reddy, A. R. Rao, and S. Sreenath, Int. J. Non-linear Mech. **42**, 1153 (2007).
[28] S. Srinivas and M. Kothandapani, Int. Comm., Heat and Mass Transfer. **35**, 514 (2008).
[29] T. Javed, A. H. Hamid, B. Ahmed, and N. Ali, J. Korean Phy. Soc. **71**, 950 (2017).
[30] A. H. Hamid, T. Javed, B. Ahmed, N. Ali, and J. Braz, Soc. Mech. Sci. Eng. **39**, 4421 (2017).
[31] S. K. Asha and C. K. Deepa, Results in Engineering **3**, 100024 (2019).
[32] N. Imran, M. Javed, M. Sohail, and I. Tlili, Journal of Materials Research and Technology **9**, 3520 (2020).
[33] H. Vaidya, C. Rajashekhar, B. B. Divya, G. Manjunatha, K. V. Prasad, and I. L. Animasaun, Results in Physics **18**, 103295 (2020).
[34] M. Rashid, K. Ansar, and S. Nadeem, Physica A: Statistical Mechanics and its Applications **553**, 123979 (2020).
[35] M. A. Imran, A. Shaheen, El-Sayed M. Sherif, Mohammad Rahimi-Gorji, and Asiful H. Seikh, Chinese Journal of Physics **66**, 60 (2020).
[36] M. I. Khan, International Communications in Heat and Mass Transfer. **122**, 105177 (2021).
[37] K. G. Kumar, B. J. Gireesha, B. C. P. Kumara, and O. D. Makinde, Diffusion Foundations **11**, 22 (2017).
[38] M. I. Khan, S. Qayyum, S. Kadry, W. A. Khan, and S. Z. Abbas, J. Magn. **25**, 8 (2020).
[39] R. S. V. Kumar, R. J. P. Gowda, R. N. Kumar, M. Radhika, and B. C. Prasannakumara, SN Applied Sciences **3**, 384 (2021).
[40] Y. M. Chu, M. I. Khan, F. Alzahrani, and A. Hobiny, J. Magn. **25**, 577 (2020).
[41] B. M. Shankaralingappa, B. J. Gireesha, B. C. Prasannakumara, and B. Nagaraja, Waves in Random and Complex Media (2021).
[42] M. I. Khan, S. Kadry, Y. M. Chu, E. M. Kalmoun, and Z. Ali, J. Magn. **25**, 307 (2020).
[43] M. G. Reddy, M. V. V. N. L. Sudha Rani, K. Ganesh Kumar, B. C. Prasannakumar, and H. J. Lokesh, Physica A: Statistical Mechanics and its Applications **551**, 123975 (2020).
[44] M. I. Khan and F. Alzahrani, International Journal of Hydrogen Energy **46**, 1362 (2021).
[45] M. I. Khan and F. Alzahrani, Physica Scripta. **95**, 125002 (2020).